Control of Block Copolymer Microdomain Orientation from Solution using Electric Fields

Governing Parameters and Mechanisms

Alexander Böker

Lehrstuhl für Physikalische Chemie II, Universität Bayreuth, D-95440 Bayreuth, Germany

1 Introduction

As nanotechnology increasingly gains importance in daily life, the need for novel nanoscopic structures also rises exponentially. For example, to keep up with Moore's law, the packing density of integrated circuits has to increase on an almost daily basis. Considering the growing number of electronically stored data, it is also clear that novel data storage techniques have to be devised aiming to increase the information density on a hard disk. For such applications, the microstructures formed by block copolymers via their microphase separation present an ideal template for the fabrication of nanoscale patterns ranging from $10 - 100\,\mathrm{nm}$ [1].

In order to profit from the self-assembly of block copolymers into various microstructures, one has to be able to control the parameters that govern this unique self-ordering process. In addition, it would be desirable to guide self-assembly via external fields to form macroscopically oriented, highly ordered structures.

Block copolymer microphase separation has been studied extensively over the past two decades both experimentally (see Fig. 1) and theoretically [2–5]. In the phase separated state, these materials exhibit highly regular mesoscopic microdomain structures with characteristic length scales of the order of several tens of nanometers. Similar to polycrystalline materials, typically small grains of microdomains are formed, the size of which may be of the order of microns. As a consequence, although a single grain may have a highly anisotropic structure (e.g. in the case of cylindrical or lamellar structures), a bulk sample of a block copolymer typically exhibits isotropic materials properties.

Control of the orientation of a block copolymer microstructure allows the development of polymeric materials with novel and interesting properties. Anisotropic mechanical, optical, electrical or mass transport properties can be tailored by proper orientation of the block copolymer microstructure. For example, alignment of glassy microphase-separated cylinders in a rubbery

matrix gives a material with a glassy modulus along the cylindrical axis and a rubbery modulus along the transverse directions [6]. If the cylinders are made conductive, the material becomes a directional conductor [7]. Quantum dots or wires could be made from block copolymers with a spherical or cylindrical microstructure [8]. The birefringence inherent in lamellar or cylindrical block copolymers could be useful for optical applications.

To create macroscopically anisotropic materials, various techniques aiming towards macroscopic microdomain alignment have been devised. Most prominently, shear fields [9–14], temperature gradients [15] and electrical fields [16–21] have been successfully applied to orient block copolymer microdomains from melt and solution. Flow provides a strong aligning force.

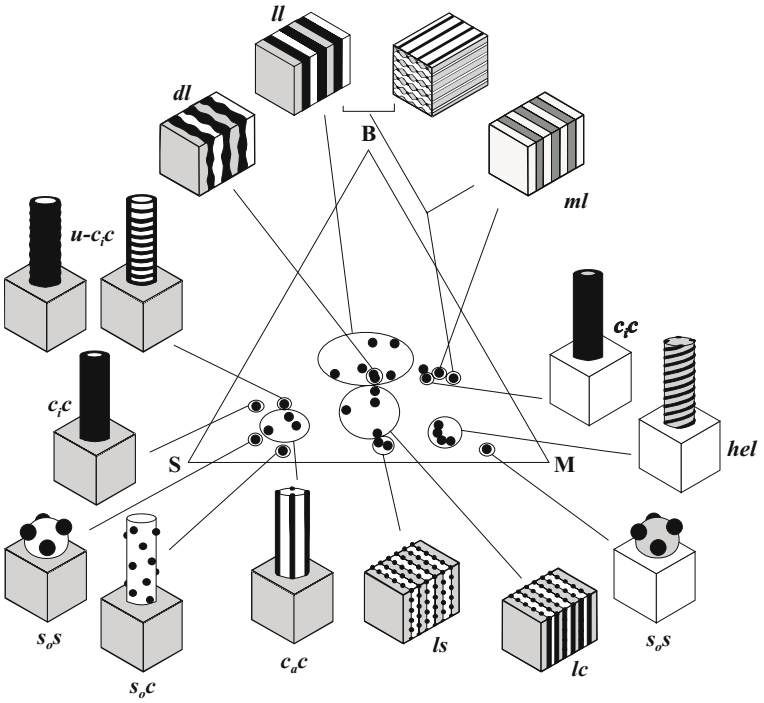

Fig. 1. Ternary phase diagram of polystyrene-*b*-polybutadiene-*b*-poly(methyl methacrylate) triblock copolymers, color according to staining with OsO_4. PS: grey, PB: black, PMMA: white [4].

However, because of boundary constraints and conditions of continuity, the potential for flow-induced orientation is limited. Electric fields provide a weaker aligning force but offer the advantage of local alignment control by application of spatially specific electric fields. For these reasons, electric fields may provide a unique pathway to new applications for block copolymers. In addition, electric field alignment is scientifically interesting because the driving force for

alignment is much simpler than that induced by flow. Studies of field alignment can be used to learn about materials properties like defect mobilities and give straightforward insight into alignment mechanisms.

Recently, the high technical potential of electric fields for microdomain alignment has attracted increasing interest [18]. It has been shown that both lamellar and cylindrical microdomain structures in polystyrene-*b*-poly(methyl methacrylate) (PS-*b*-PMMA) melts could be oriented macroscopically by virtue of a DC electric field [17, 22–26]. Due to the differences in the dielectric constants ($\Delta\varepsilon = \varepsilon_\mathrm{A} - \varepsilon_\mathrm{B}$) of the blocks ($\varepsilon_\mathrm{PS} \approx 2.6$, $\varepsilon_\mathrm{PMMA} \approx 3.6$) [27], the microdomains tend to orient parallel to the electric field vector, thereby lowering the free energy of the system. The associated electric field-induced driving force is proportional to $\frac{(\varepsilon_\mathrm{A}-\varepsilon_\mathrm{B})^2}{\langle\varepsilon\rangle}E^2$ [28]. Cylindrical microdomains can in principle be aligned along the field vector resulting in a single monodomain (i.e. a block copolymer *single crystal*). In a lamellar microdomain structure, on the other hand, all lamellar orientations containing the electric field vector within the lamellar planes are energetically equivalent. Therefore, the electric field is expected to at best favor the sub-set of lamellar orientations with the lamellar normal pointing perpendicular to the field.

So far most experiments using electric fields have been conducted in the melt. Due to the high melt viscosities, they are limited with respect to the molecular weight of the copolymers and the size of the macroscopic regions to be oriented ($M_w \approx 74\,000$ g/mol for thin films of thickness 1 μm [29]; $M_w \approx 37\,000$ g/mol for samples of thickness 2 mm [17, 22]). In addition, temperatures close to the decomposition temperature and electric field strengths of up to 25 kV/mm are required to achieve high degrees of orientation. These limitations render the orientation of higher molecular weight copolymers or copolymers of more complex architectures (multiblock copolymers, star copolymers, etc.) rather difficult if not impossible, since their melt viscosities easily exceed the values faced in the investigations quoted above. Given the increasing interest in complex block copolymer structures and their technical potential [1], it is therefore desirable to explore alternative approaches, which circumvent the above limitations. One of these alternatives is the large scale alignment of block copolymer microdomains from concentrated polymer solutions due to the high polymer chain mobility. The mechanisms and kinetics can be investigated using small-angle X-ray scattering. This technique yields detailed insight into the microscopic structure and microdomain order with a high time resolution on the order of milliseconds. The details of this procedure as well as the parameters governing the electric field-induced orientation will be discussed in the following.

2 Experimental

2.1 Sample Preparation and Capacitor Setup

The block copolymers were synthesized by sequential living anionic polymerization [30,31]. In the following sections, we will employ different block copolymers such as polystyrene-*b*-poly(2-hydroxyethyl methacrylate)-*b*-poly(methyl methacrylate), polystyrene-*b*-poly(methyl methacrylate), and polystyrene-*b*-polyisoprene. We refer to the block copolymers as $S_{47}H_{10}M_{43}{}^{82}$, $S_{49}M_{51}{}^{100}$, $S_{50}I_{50}{}^{80}$ and $S_{50}I_{50}{}^{100}$, respectively with the subscripts denoting the weight fractions of the respective blocks and the superscript indicating the number-averaged molecular weight in kg/mol. All polymers are rather monodisperse with polydispersities $M_w/M_n \approx 1.04$.

The alignment experiments were perfomed in a home-built closed capacitor with gold electrodes (electrode spacing: $0.3 - 4$ mm, sample depth: 5 mm; Fig. 2). A DC voltage between 0.25 and 3 kV/mm was applied across the electrodes resulting in an electric field perpendicular to the X-ray beam direction. Block copolymer solutions with polymer concentrations between 30 and 70 wt.% were investigated with in-situ Synchrotron-SAXS at the ID2 beamline at the European Synchrotron Radiation Facility (ESRF, Grenoble, France).

2.2 Synchrotron Small-Angle X-Ray Scattering (Synchrotron-SAXS)

The diameter of the X-ray beam was 100 μm. The photon energy was set to 12.5 keV. SAXS patterns were recorded with a two-dimensional CCD camera located at a distance of 10 m from the sample within an evacuated flight tube. The detector can monitor up to 120 frames ($1\,024 \times 1\,024$ pixels) at a rate of 10 frames per second. Prior to data analysis, background scattering was subtracted from the data and corrections were made for spatial distortions and for the detector efficiency.

2.3 Calculation of Order Parameters from SAXS Data

As will become clear from the experimental observations described in the following sections, domain alignment is induced by two competing external fields of different symmetry, i.e. the interfacial field between polymer solution and electrode surface and the electric field, respectively. To quantify the alignment, we calculate the order parameter P_2 by integrating the scattering intensity from $\varphi = 0°$ to 360°:

$$P_2 = \frac{3\left\langle \cos^2 \varphi \right\rangle - 1}{2} \tag{1}$$

with

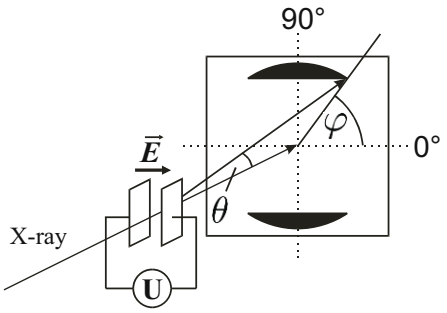

Fig. 2. Sketch of the experimental setup for in-situ synchrotron small angle X-ray scattering (SAXS) experiments at the ID2 beamline at the European Synchrotron Radiation Facility (ESRF) in Grenoble, France. Reprinted with permission from *Phys. Rev. Lett.* [21]. Copyright (2002) The American Physical Society.

$$\left\langle \cos^2 \varphi \right\rangle = \frac{\int_0^{2\pi} d\varphi \left(I_q(\varphi) \cos^2 \varphi \left| \sin \varphi \right| \right)}{\int_0^{2\pi} d\varphi \left(I_q(\varphi) \left| \sin \varphi \right| \right)} \tag{2}$$

Depending on the position of the maxima of the scattering intensity the calculation yields two different ranges of the order parameter. For lamellar alignment parallel to the electrodes (maximum at $\varphi = 0°$), P_2 ranges from 0 to 1 with $P_2 = 1$ corresponding to perfect lamellar alignment where all lamellar normals are oriented perpendicular to the surfaces, i.e. electrodes. For alignment of the lamellae along the electric field direction (maximum at $\varphi = 90°$), P_2 ranges from 0 to -0.5 with $P_2 = -0.5$ corresponding to the case where all lamellae are aligned parallel to the electric field vector, however, with the lamellar normals being isotropically oriented in the plane of the electrodes.

In order to quantify the orientation kinetics, the orientational order parameter P_2 was calculated for each single scattering pattern acquired during the course of the experiment. The behavior of P_2 as a function of time t has been fitted by a single exponential as described by:

$$P_2(t) = P_{2,\infty} + (P_{2,0} - P_{2,\infty})\, e^{-\frac{t}{\tau}} \tag{3}$$

with $P_{2,0}$ and $P_{2,\infty}$ being the limiting values of the order parameter before application of the electric field and at later times, respectively, and τ being the time constant.

2.4 Computer Simulation

We employ the dynamic self-consistent field theory, which describes the dynamic behavior of each molecule (modeled as Gaussian chains) in the mean-field of all other molecules [32,33]. The phase separation can be monitored by

the scalar order parameter $\Psi(\boldsymbol{r}, t)$, which is the normalized deviation of the density of a polymer component from its average value. In the case of an incompressible diblock copolymer melt the system is described by only a single order parameter. Simulating a diblock copolymer solution requires an extra order parameter for the solvent; however, we use a simplified model with only one order parameter in the present study. It was shown theoretically that a block copolymer melt can serve as a good approximation to describe general features of phase behavior of concentrated block copolymers solutions with nonselective good solvents [34]. As we have shown recently, this description is well justified and gives an excellent agreement with experiments in the case of a nonselective or almost nonselective solvent [35]. The time evolution of the order parameter in the simplest case follows a diffusion type equation [36]

$$\dot{\Psi} = M\,\nabla^2\mu + \eta \tag{4}$$

with the constant mobility M, and the thermal noise η [33]. The chemical potential in the presence of an electric field $\boldsymbol{E}$ has the form $\mu = \mu^0 - \left(\frac{\partial\,\varepsilon}{\partial\Psi}\right)_T \cdot \frac{E^2}{8\pi}$ [28], where μ^0 is the chemical potential in the absence of the electric field, and ε is the dielectric constant of the polymeric material, which can be approximated as $\varepsilon \approx \varepsilon_0 + \varepsilon_1\,\Psi$ for small Ψ. The electric field $\boldsymbol{E}$ inside the material deviates from the applied electric field $\boldsymbol{E}_0 = (0, 0, E_0)$ and can be written via an auxiliary potential as $\boldsymbol{E} = \boldsymbol{E}_0 - \nabla\varphi$. The potential is related to Ψ via the Maxwell equation $\mathrm{div}\,\varepsilon\boldsymbol{E} = 0$. Keeping only leading terms, one can rewrite (4) in the form [37]

$$\dot{\Psi} = M\,\nabla^2\mu^0 + \alpha\,{\nabla_z}^2\,\Psi + \eta \tag{5}$$

with

$$\alpha \equiv M\,{E_0}^2\,\frac{{\varepsilon_1}^2}{4\pi\,\varepsilon_0} \tag{6}$$

The chemical potential without the electrostatic contribution μ^0 is calculated using self-consistent field theory for the ideal Gaussian chains with the mean field interactions between copolymer blocks A and B, described by a parameter $\varepsilon_{\mathrm{AB}}$ [37].

The model system we study in the following is a symmetric A_4B_4- copolymer melt. The simulations have been performed in a two-dimensional box with 256 x 256 grid points and periodic boundary conditions [32]. For the simulations, the electric field strength is parameterized by $\tilde{\alpha} \equiv \alpha\,/\,(kT\,M\,v)$ [37,38], where v is a polymer chain volume. The samples were shear-aligned with the dimensionless shear rate $\tilde{\dot{\gamma}} = 0.001$, for details please see [39].

3 Role of the Dielectric Contrast

As has been pointed out in the introduction to this chapter, the difference in the dielectric constants of the blocks $\Delta\varepsilon = \varepsilon_{\mathrm{A}} - \varepsilon_{\mathrm{B}}$ is a major factor

determining the electric field-induced microdomain orientation. Therefore, in this section, we study the orientation behavior of a $S_{49}M_{51}{}^{100}$ diblock and a $S_{47}H_{10}M_{43}{}^{82}$ triblock copolymer which exhibit different dielectric contrasts between the polystyrene and methacrylic block.

3.1 Experimental Comparison of the Diblock ($\mathbf{S_{49}M_{51}{}^{100}}$) and the Triblock ($\mathbf{S_{47}H_{10}M_{43}{}^{82}}$)

Structure Formation in Solution

As an external electric field can only align a microphase-separated structure, we studied the structure evolution of the $S_{49}M_{51}{}^{100}$ diblock and $S_{47}H_{10}M_{43}{}^{82}$ triblock copolymer in tetrahydrofurane (THF) solutions with SAXS as a function of polymer concentration w_p. Starting from $w_\mathrm{p} = 30$ wt.% and increasing w_p stepwise by 2.5 wt.% up to 60 wt.% we aimed to determine the order- disorder concentration w_ODT of the two block copolymer systems. From these measurements we find that for the $S_{49}M_{51}{}^{100}$ diblock copolymer the w_ODT is located at around 53 wt.%. For the $S_{47}H_{10}M_{43}{}^{82}$ triblock copolymer, we locate w_ODT at around 40 wt.%. Obviously, the presence of the PHEMA middle block leads to an increased incompatibility between the blocks and thereby to a lower order-disorder concentration. As a consequence, the viscosity of solutions just above the order-disorder concentration w_ODT is significantly lower for the $S_{47}H_{10}M_{43}{}^{82}$ as compared to the $S_{49}M_{51}{}^{100}$ block copolymer.

Reorientation Behavior

After sample preparation and prior to electric field exposure, all phase-separated solutions exhibit a distinctly anisotropic scattering pattern with maxima located at $\varphi = 0°$ and 180° (Fig. 3a). This pattern indicates alignment of the lamellae parallel to the electrodes. Such an alignment can be caused both by preferential interaction of polystyrene with the gold surfaces and by shear forces acting on the highly viscous solutions during the filling of the capacitor with a syringe [40]. As the lowest possible concentration (and thus viscosity) to give a phase separated polymer solution for the $S_{49}M_{51}{}^{100}$ diblock copolymer system was found at 53 wt.% in THF, the system only exhibits very slow reorientation of the microdomains at a field strength of 2 kV/mm (see Fig. 4b). We note that the data shown here represent the fastest possible realignment kinetics achievable for the $S_{49}M_{51}{}^{100}$ system, as with increasing polymer concentration, the viscosity immediately dominates the process, rendering the reorientation impossible. Obviously, above w_ODT the force acting on the lamellae is not sufficient to lead to significant reorientation [20], rearranging the microstructure in a highly viscous solution. In the triblock copolymer case a different behavior is observed. As soon as an electric field of 1 kV/mm is applied to a 40 wt.% solution, the scattering pattern changes significantly. The peaks at $\varphi = 0°$ and 180° decrease and new scattering maxima at $\varphi = 90°$ and 270° grow with time (Figs. 3a–c).

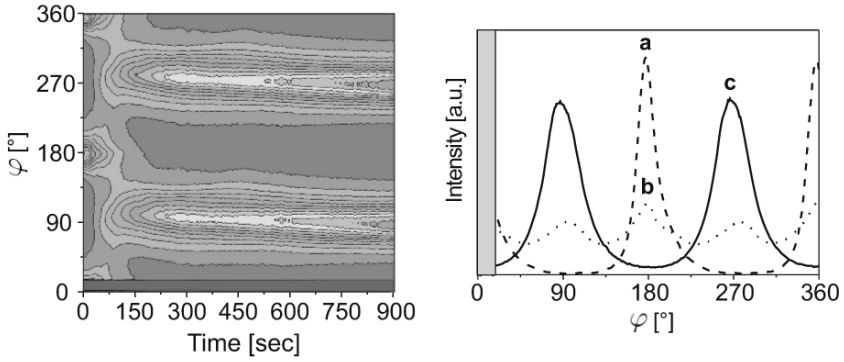

Fig. 3. (Left) Time development of the azimuthal angular dependence of the scattering intensity of a 40 wt.% solution of $S_{47}H_{10}M_{43}{}^{82}$ in THF at 1 kV/mm (electrode spacing: 1 mm). The lighter regions represent the highest intensity and the darker regions indicate the lowest scattering intensity. (Right) Azimuthal scattering intensity at (**a**) $t = 0$ sec, (**b**) $t = 100$ sec, (**c**) $t = 900$ sec. Reprinted with permission from *Polymer* [41]. Copyright (2005) Elsevier Ltd.

Concentration Dependence

The kinetics of the microdomain alignment was followed within a narrow concentration window between the order-disorder concentration $w_{\mathrm{ODT}}(\approx 40\,\mathrm{wt.\%})$ and $w_{\mathrm{p}} = 50\,\mathrm{wt.\%}$ for the $S_{47}H_{10}M_{43}{}^{82}$ block copolymer. The orientational order parameter P_2 was calculated for each azimuthal angular scattering intensity distribution obtained from the X-ray scattering images during the reorientation process using (1). Plots of P_2 versus time yield an exponential dependence, which was fitted according to (3) to give the time constants τ. As can be seen from Fig. 4 and Table 1, the time constants for the reorientation process at 1 kV/mm are in the range of some minutes (1.5 minutes for 40 wt.% and almost 6 minutes for 45 wt.%, respectively). At concentrations above 45 wt.% no electric field induced orientation could be detected. Moreover, at 45 wt.% (Fig. 4b) the process is slowed down significantly at an incomplete degree of alignment ($P_2 = 0.28$), which can only be overcome by increasing the field strength. At a polymer concentration of 50 wt.%, within the experimental time window of several minutes, no microdomain orientation could be achieved at field strengths as high as 6 kV/mm. The results of the exponential fits are summarized in Table 1. The single exponential fit works quite well for all concentrations studied, as can be seen from the low χ^2 values. At a sufficiently high electric field strength, P_2 reaches about the same limiting values $P_{2,\infty} = -0.25 \pm 0.02$ independent of concentration.

We note that the behavior displayed in Fig. 4 results from a delicate balance between an increase of both the driving force for reorientation (i.e. a larger dielectric contrast) and the viscous retardation as the polymer concentration is increased [21]. The exact behavior is difficult to predict; however,

Table 1. Time constants τ of the reorientation of $S_{47}H_{10}M_{43}{}^{82}$ at different polymer concentrations and different electric field strengths E obtained from least squares fits using (3) (electrode spacing: 1 mm).

Concentration [wt.%]	E [kV/mm]	τ [sec]	$P_{2,\infty}$	χ^2 [10^{-4}]
40	1	89	-0.26	3.8
45	1	348	0.28	0.5
45	2	157	-0.23	1.4
45	3	151	-0.27	0.6

the data shown in Fig. 4 and Table 1 indicate that in the particular system studied here the increase in viscosity dominates over the increase of the driving force. Therefore, the reorientation process slows down with increasing polymer concentration. For a sufficiently high electric field strength the viscosity only influences the kinetics but not the final degree of order ($P_{2,\infty}$), which is consistent with previous dielectric relaxation spectroscopy measurements on the realignment of side chain liquid crystalline polymers in their liquid-crystalline state induced by a DC electric field [42].

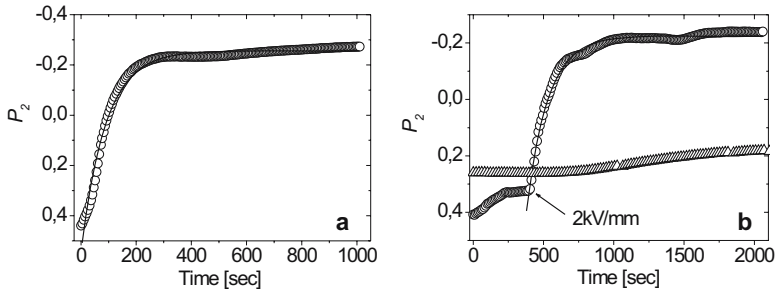

Fig. 4. Evolution of orientational order parameter P_2 with time (for orientation parallel to the electric field vector). (**a**) 40 wt.% solution of $S_{47}H_{10}M_{43}{}^{82}$ in THF at 1 kV/mm, (**b**) 45 wt.% solution of $S_{47}H_{10}M_{43}{}^{82}$ in THF at 1 kV/mm and 2 kV/mm (◯). For comparison, the data for a 53 wt.% solution of $S_{49}M_{51}{}^{100}$ in THF at 2 kV/mm is added (△). The solid lines represent least squares fits to the data (electrode spacing: 1 mm) according to (3). Reprinted with permission from *Polymer* [41]. Copyright (2005) Elsevier Ltd.

If this procedure was to be used for the preparation of macroscopically aligned bulk samples via solution casting in the presence of an electric field, the alignment process should be faster than the time needed for solvent evaporation. From the above results we conclude that concentrations between 40 wt.%

and 45 wt.% are suitable for the preparation of dried bulk samples from solution. Figure 5 shows the feasibility of such a process for the $S_{47}H_{10}M_{43}{}^{82}$ block copolymer system. Using a home-built capacitor which allows application of an electric DC field during film formation by solvent casting, a melt sample of 1 mm thickness (dried in the presence of an electric field of 2 kV/mm) was prepared from a 25 wt.% solution in chloroform (comparable to 40 wt.% in THF). SAXS investigations yield an orientational order parameter of $P_2 = -0.4$. Here we note that a similar process with the $S_{49}M_{51}{}^{100}$ diblock copolymer system did not yield anisotropic bulk samples. In the following, we shall try to give some theoretical evidence to support the experimental facts reported above.

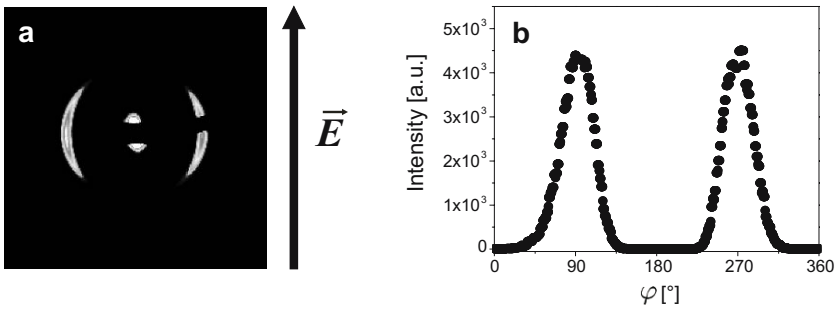

Fig. 5. (**a**) 2D-SAXS pattern of a film cast in the presence of a DC electric field ($E = 2\,\mathrm{kV/mm}$). The lamellae are oriented preferentially along the field direction. (**b**) Azimuthal intensity distribution at the first order reflection ($P_2 = -0.4$). Reprinted with permission from *Polymer* [41]. Copyright (2005) Elsevier Ltd.

3.2 Theoretical Comparison of the Diblock ($S_{49}M_{51}{}^{100}$) and the Triblock ($S_{47}H_{10}M_{43}{}^{82}$)

Here, we will consider electrostatic arguments to discuss the different behavior observed for the PS-*b*-PMMA ($S_{49}M_{51}{}^{100}$) and the PS-*b*-PHEMA-*b*-PMMA ($S_{47}H_{10}M_{43}{}^{82}$) diblock and triblock copolymers with significantly different dielectric contrasts.

We aim to estimate the electrostatic energies involved in the process of microdomain orientation. As indicated by differential scanning calorimetry (DSC), rheological and transmisssion electron microscopy (TEM) experiments, we anticipate that the PHEMA and the PMMA form a mixed phase. This leads us to treat the triblock copolymer as an AB diblock copolymer with the following composition: A: 47 wt.% PS ($\varepsilon_\mathrm{A} = 2.6$) and B: 53 wt.% methacrylic blocks ($\varepsilon_\mathrm{B} = 0.81\,\varepsilon_\mathrm{PMMA} + 0.19\,\varepsilon_\mathrm{PHEMA} = 4.6$; with $\varepsilon_\mathrm{PMMA} = 3.6$ and $\varepsilon_\mathrm{PHEMA} = 8.9$ [43]). Thus the dielectric contrast for the $S_{47}H_{10}M_{43}{}^{82}$ tri-

block amounts to $\Delta\varepsilon = 2.0$. For the $S_{49}M_{51}{}^{100}$ diblock copolymer the dielectric contrast only yields $\Delta\varepsilon = 1.0$.

As chloroform ($\varepsilon_{CHCl_3} = 4.8$) and THF ($\varepsilon_{THF} = 7.8$) are fairly non-selective solvents for the two main components, PS and PMMA, we expect a similar swelling behavior leading merely to a dilution effect with respect to the dielectric constants of each block. Therefore, with increasing solvent content in the films, the difference of the dielectric constants is reduced and the electrostatic driving force for an alignment of the lamellae parallel to the field is expected to decrease [26]. As has been pointed out by Amundson et al. [17] with respect to melts of PS-*b*-PMMA block copolymers this force is already small, so it is remarkable that its decrease still leaves a sufficient driving force to allow for preferential alignment of the microdomains.

To estimate the driving forces for domain alignment as a function of solvent volume fraction ϕ_s, we calculate the electric energy per volume W, which is stored in a capacitor for an open setup which allows for solvent evaporation (including a layer of air in the system) and a closed system as used for the in-situ SAXS studies. The model relies on two major assumptions: The dielectric constant of a mixture ε_{mix} of polymer ε_p and solvent ε_s is assumed to depend linearly on the solvent volume fraction ϕ_s:

$$\varepsilon_{mix} = \phi_s\,\varepsilon_s + (1-\phi_s)\,\varepsilon_p \tag{7}$$

We further disregard any influence of the solvent on the partial molar volume of the polymer, i.e. the volumes of polymer V_p and solvent V_s simply add:

$$V_{mix} = V_p + V_s \tag{8}$$

Film formation in the open capacitor under the influence of an external electric field may result in significant thickness undulations which eventually lead to the formation of column-like protrusions that connect both electrodes [20,44]. Therefore, we have identified four basic geometries to describe the open system, corresponding to a perpendicular ($W_{\perp,col}$, $W_{\perp,flat}$) and parallel ($W_{\parallel,col}$, $W_{\parallel,flat}$) alignment of the microdomains with respect to the electric field and to a formation of columns ($W_{\perp,col}$, $W_{\parallel,col}$) and a flat film ($W_{\perp,flat}$, $W_{\parallel,flat}$), respectively (Fig. 6a). In the case of the closed capacitor, the two perpendicular ($W_{\perp,col}, W_{\perp,flat} = W_{\perp}$) and two parallel ($W_{\parallel,col}, W_{\parallel,flat} = W_{\parallel}$) cases are equivalent.

We calculate the energy W stored within the electric field of the capacitor according to

$$W = \frac{1}{2}\int \boldsymbol{E}\boldsymbol{D}\,dV \tag{9}$$

with $\boldsymbol{E}$ being the electric field and $\boldsymbol{D}$ the displacement field.

In contrast to the dielectric displacement $\boldsymbol{D}$, the electric field $\boldsymbol{E}$ along the z-direction of the capacitor is not uniform for the models, which incorporate a layered structure ($W_{\perp,flat}$ and $W_{\perp,col}$). This is due to the fact that the component of the electric field perpendicular to the interface between two materials

is not continuous, but the one of the displacement field is: $\boldsymbol{D}_{\perp 1} = \boldsymbol{D}_{\perp 2}$ but $\boldsymbol{E}_{\perp 1} \neq \boldsymbol{E}_{\perp 2}$. Additionally $\boldsymbol{E}_{\mathrm{i}} = \boldsymbol{D}_{\mathrm{i}}/\varepsilon_{\mathrm{i}}$ and the applied voltage $U = \int \boldsymbol{E}\, dz$, which means that as soon as air is present as a layer in the capacitor with the applied voltage U, the electric field in both polymer layers is reduced. This leads effectively to a reduced energy stored inside the capacitor and to a reduced alignment of the block copolymer in the thinner parts of the sample. We are well aware of the fact that our calculations neglect the existence of interfacial boundary regions in concentrated polymer solutions. Therefore, the results may represent an approximation to the upper limit of the real energetic situation.

In order to allow for a straightforward comparison between the open and closed system, we used chloroform for both calculations. Similar calculations using THF as solvent confirmed a qualitative agreement with the results obtained for the chloroform case.

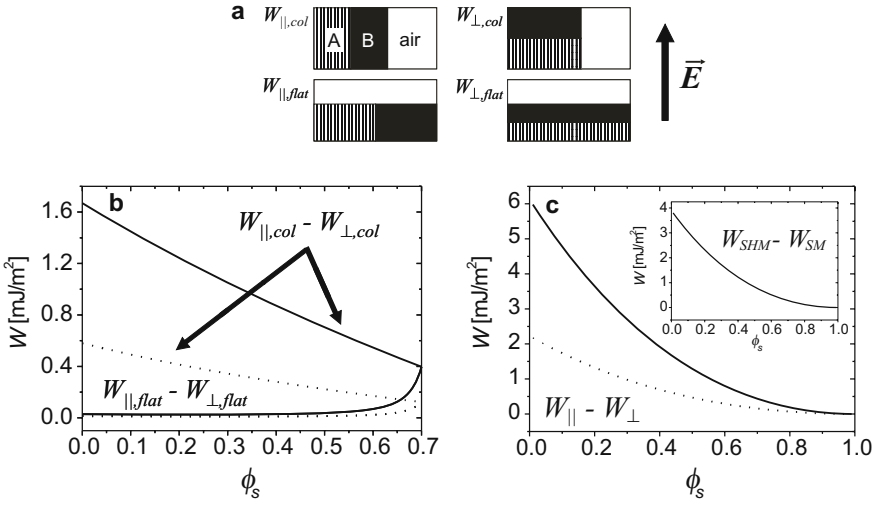

Fig. 6. (**a**) Four basic geometries of lamellar orientation in an open capacitor. (**b**/**c**) Free energy calculations for the lamellar orientation in an open and closed capacitor filled with polymers A and B at geometries shown in (**a**). (**b**) Energy difference between the two orientations for columns ($W_{\parallel,col} - W_{\perp,col}$) and for a flat film ($W_{\parallel,flat} - W_{\perp,flat}$) in an open capacitor which allows for solvent evaporation: $S_{47}H_{10}M_{43}{}^{82}$ (—) and $S_{49}M_{51}{}^{100}$ ($\cdots$) block copolymers in $CHCl_3$. (**c**) Difference in calculated energy between the orientations parallel and perpendicular to the electric field vector within a closed capacitor filled with $S_{47}H_{10}M_{43}{}^{82}$ (—) and $S_{49}M_{51}{}^{100}$ ($\cdots$) in $CHCl_3$ as a function of solvent volume fraction ϕ_s (geometries as depicted in (**a**) but with no air layer). The inset shows the overall energy difference between the two polymer systems. In all calculations the field strength is 2 kV/mm. Reprinted with permission from *Polymer* [41]. Copyright (2005) Elsevier Ltd.

Figure 6b shows the difference in energy stored per volume within an open capacitor filled with 15 vol.% polymer A (with $\varepsilon_A = 2.6$ for PS phase) and 15 vol.% polymer B (with $\varepsilon_B = 4.6$ for PHEMA/PMMA mixed phase (—) and $\varepsilon_B = 3.6$ for pure PMMA phase ($\cdots$)) as a function of chloroform volume fraction ϕ_s ($\varepsilon_{CHCl_3} = 4.8$), corresponding to the four basic geometries, at a field strength of 2 kV/mm. The curve $W_{\parallel,col} - W_{\perp,col}$ as well as the curve $W_{\parallel,flat} - W_{\perp,flat}$ converge at a solvent volume fraction of 70 vol.% (which is the starting point of our solvent casting experiment), because at this point the capacitor is completely filled and the respective geometries are equivalent.

Besides the fact that for the SHM as well as the SM system the difference in energy between the two orientations in columns ($W_{\parallel,col} - W_{\perp,col}$) is larger than for flat films ($W_{\parallel,flat} - W_{\perp,flat}$), the overall energetic difference is about three times higher for the SHM than for the SM system.

In Fig. 6c, we show the results of the calculations for the difference in energy between the orientations parallel and perpendicular to the electric field vector within a closed capacitor filled with different solutions of our model block copolymers in chloroform with $\varepsilon_A = 2.6$ and $\varepsilon_B = 4.6$ (resembling $S_{47}H_{10}M_{43}{}^{82}$, full line) and with $\varepsilon_A = 2.6$ and $\varepsilon_B = 3.6$ (resembling $S_{49}M_{51}{}^{100}$, dotted line) as a function of solvent volume fraction ϕ_s at a field strength of 2 kV/mm. Compared to an open capacitor the system stores at least two times more energy at any given solvent volume fraction up to 80 vol.%. The inset depicts the overall energy difference between the above described cases, i.e. the aligned triblock terpolymer lamellae always allow the capacitor to store more energy than the diblock system.

When we compare the two situations described above, we find that: (i) the closed system stores more energy per volume, (ii) the difference in energy between the two orientations ($W_\parallel - W_\perp$) is always higher for the experimentally relevant concentrations in the closed capacitor, and (iii) in all cases, the SHM system is clearly electrostatically favored as it allows the capacitor to store more energy per volume. Therefore, from our experimental findings, we may conclude that, if the electric field induced orientation of a block copolymer does not work in the closed capacitor, it will neither function in the open system, as the energetic difference is always larger for the closed capacitor setup. Furthermore, the incorporation of the high dielectric constant PHEMA middle block into the PS-*b*-PMMA diblock copolymer is the key to increasing the electrostatic driving force of the alignment process in order to create a well-performing methacrylate-based block copolymer system for electric field-induced alignment from *solution*.

Moreover, the PHEMA block enhances the microphase-separation in the block copolymer solutions compared to the PS-*b*-PMMA system. While the w_{ODT} for the $S_{49}M_{51}{}^{100}$ block copolymer is found at around 53 wt.%, the PHEMA containing block copolymer already microphase-separates at $w_p \approx 40$ wt.%. Therefore, in the latter case, the viscosity of the phase-separated solution is considerably smaller, which promotes the kinetics of the ordering process induced by the small electric force. On the other hand,

a lower polymer concentration also reduces the effective field strength and driving force in the capacitor as shown in Figs. 6b/c.

To this point, we can not decide definitely if in this particular system enhanced phase separation or the increased dielectric contrast between the blocks is more important for the electric field-induced ordering process to function. So far, all results point to a delicate balance between both parameters.

4 Concentration and Temperature Dependence of Orientation Mechanisms and Kinetics

In this section, we describe in-situ synchrotron small-angle X-ray scattering (Synchrotron-SAXS) investigations aiming to follow the kinetics of electric field-induced microdomain reorientation in concentrated block copolymer solutions, and thus, to elucidate the underlying microscopic mechanisms. As a model system, we employ a lamellae-forming polystyrene-*b*-polyisoprene diblock copolymer ($S_{50}I_{50}{}^{80}$) dissolved in toluene. We discuss the influence of the polymer concentration and the temperature on the reorientation behavior.

In addition to the experiments, we performed computer simulations based on dynamic density functional theory (DDFT).

4.1 Structure Formation in Solution

First, we investigated the ordering behavior of the block copolymer solutions in the absence of an electric field. At room temperature, we found an order-disorder transition (ODT) at $w_{\mathrm{ODT}} \approx 35\,\mathrm{wt.\%}$, above which a well defined lamellar microdomain structure is developed. A characteristic lamellar spacing of $d_{\mathrm{SAXS}} = 39\,\mathrm{nm}$ is found at $w_{\mathrm{p}} = 35\,\mathrm{wt.\%}$, which increases smoothly with increasing polymer concentration. After filling the capacitors with the polymer solution, the microdomain structure appears to be highly oriented parallel to the electrodes. This can be seen from the two-dimensional SAXS pattern displayed in Fig. 7a, which shows two distinct peaks around $\varphi = 0°$ and $\varphi = 180°$.

When an electric field is applied across the two electrodes, the scattering pattern changes significantly. As can be seen from the snapshots taken at different times, the anisotropic pattern first turns into an isotropic ring of weak intensity (Fig. 7b, $t = 6\,\mathrm{sec}$) before two distinct peaks are formed around $\varphi = 90°$ and $\varphi = 270°$ at later times (Fig. 7c, $t = 34\,\mathrm{sec}$). The complete set of data is displayed in Fig. 8a, where the intensity of the (1 0 0) peak is plotted as a function of φ for increasing time t. Clearly an almost complete destruction of the initial peaks is seen at early times followed by the buildup of new peaks around $\varphi = 90°$ and $\varphi = 270°$.

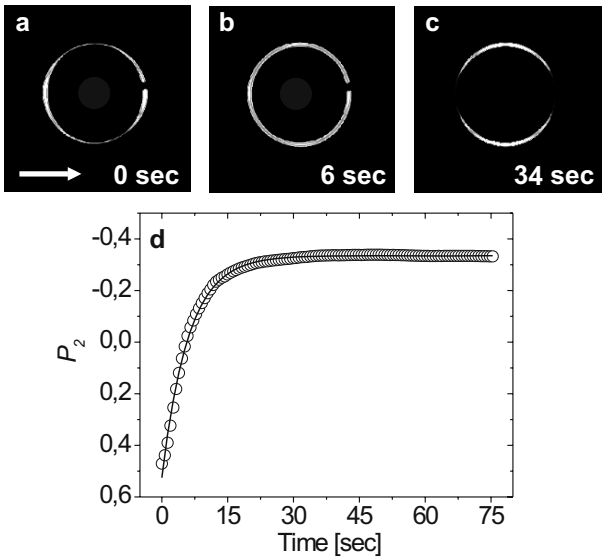

Fig. 7. Two-dimensional SAXS patterns of a 35 wt.% solution of the $S_{50}I_{50}{}^{80}$ diblock copolymer in toluene taken at 25°C prior to (**a**) and after application of an electric field ($E = 1\,\mathrm{kV/mm}$) (**b**,**c**). (**d**) Time dependence of the orientational order parameter P_2. The solid line is a least squares fit to the data according to (3) with $P_{2,0} = 0.52$, $P_{2,\infty} = -0.32$, and $\tau = 5\,\mathrm{sec}$. The arrow indicates the direction of the electric field vector. Reprinted with permission from *Macromolecules* [45]. Copyright (2003) American Chemical Society.

To quantify the kinetics of the orientation process, the orientational order parameter $P_2(t)$ was calculated from the 2D SAXS images according to (3). Using a single exponential fit, we can determine the time constant of the reorientation process (Fig. 7d).

4.2 Kinetics of Microphase Orientation

For the effective preparation of highly anisotropic melt block copolymer samples via solvent casting in the presence of an external electric field, it is important to find an optimum set of parameters (i.e. degree of swelling of the block copolymer domains, electric field strength, and temperature), which combines a maximum chain mobility (i.e. fast kinetics) with the highest possible polymer concentration. In short, the reorientation process should be faster than the rate of solvent evaporation during preparation of bulk samples from solution, i.e. it should be completed before the bulk structure "freezes".

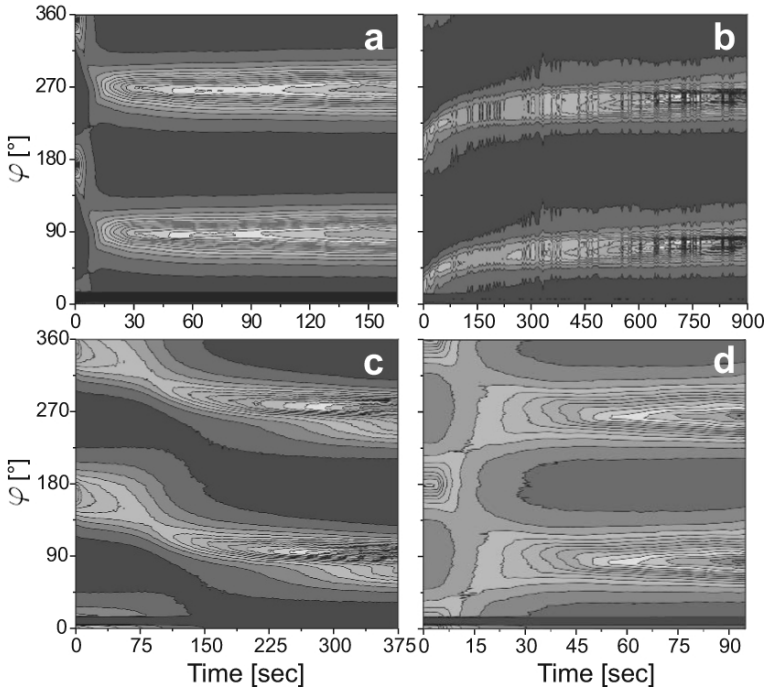

Fig. 8. Time development of the scattering intensity as a function of the azimuthal angle φ in the presence of an electric field of strength $E = 1\,\mathrm{kV/mm}$ for different polymer concentrations and temperatures. (**a**) $w_\mathrm{p} = 35\,\mathrm{wt.\%}$, $T = 25^\circ\mathrm{C}$; (**b**) $w_\mathrm{p} = 50\,\mathrm{wt.\%}$, $T = 25^\circ\mathrm{C}$; (**c**) $w_\mathrm{p} = 47.5\,\mathrm{wt.\%}$, $T = 27^\circ\mathrm{C}$; (**d**) $w_\mathrm{p} = 47.5\,\mathrm{wt.\%}$, $T = 80^\circ\mathrm{C}$. Reprinted with permission from *Phys. Rev. Lett.* [21]. Copyright (2002) The American Physical Society.

Concentration Dependence

In a first series of experiments, we studied the reorientation kinetics as a function of polymer concentration, starting from $w_\mathrm{p} = 30\,\mathrm{wt.\%}$ and increasing w_p stepwise by $1\,\mathrm{wt.\%}$ up to $35\,\mathrm{wt.\%}$ and then by steps of $2.5\,\mathrm{wt.\%}$ to higher polymer concentrations. The electric field strength E was kept constant at $E = 1\,\mathrm{kV/mm}$ at a capacitor spacing of $2\,\mathrm{mm}$. Starting from w_ODT, the scattering patterns changed following the behavior shown in Fig. 7 so that time constants $\tau(w_\mathrm{p})$ could be determined from the time evolution of P_2 as shown in Fig. 9. Above $w_\mathrm{p} = 50\,\mathrm{wt.\%}$, however, the reorientation process was so slow ($\tau \approx 5\,\mathrm{min}$) so that we limited our study to polymer concentrations between 34.5 and $50\,\mathrm{wt.\%}$.

The results of the exponential fits and the increase of the time constant τ with increasing polymer concentration are summarized in Table 2. The single exponential fit works quite well for all concentrations studied, as can be seen from the low χ^2 values. The time constants vary from $\tau = 0.8\,\mathrm{sec}$

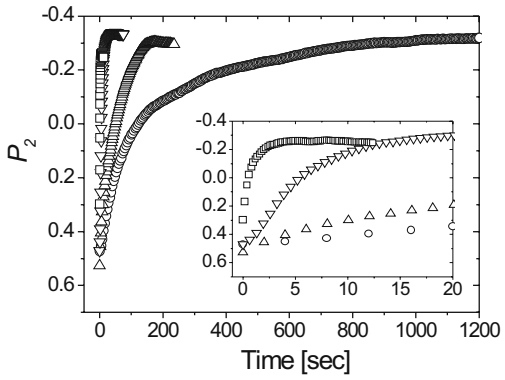

Fig. 9. Evolution of the orientational order parameter P_2 with time for different concentrations at 1 kV/mm ($\square$ = 34.5 wt.%, $\triangledown$ = 37.5 wt.%, $\triangle$ = 42.5 wt.%, $\bigcirc$ = 50 wt.% (electrode spacing: 2 mm). Reprinted with permission from *Macromolecules* [45]. Copyright (2003) American Chemical Society.

for the very fast processes at 34.5 wt.% to more than 3 minutes ($\tau = 192$ sec) for the 50 wt.% solution. In addition, within some 10% scatter P_2 reaches about the same limiting values $P_{2,\infty} = -0.3 \pm 0.03$ independent of polymer concentration. Therefore, we can conclude that the polymer concentration only influences the rate but not the final degree of orientation. We note that the behavior displayed in Fig. 9 results from a delicate balance between an increase of both the driving force for reorientation (i.e. a larger dielectric contrast) and the viscous drag as the polymer concentration is increased [21]. The exact behavior is difficult to predict; however, the data shown in Fig. 9 and Table 2 indicate that in the particular system studied here, just as found for the $S_{47}H_{10}M_{43}{}^{82}$ block copolymer, the increase in viscosity dominates over the increase of the driving force. Therefore, the reorientation process slows down with increasing polymer concentration.

Interestingly, along with an overall slowing down of the reorientation at higher polymer concentration, the microscopic mechanism of microdomain reorientation changes as a function of the polymer concentration. This can be seen in Figs. 8a/b, where we compare the time dependence of the scattering patterns for the limiting polymer concentrations, $w_p = 35$ wt.% and $w_p = 50$ wt.%, respectively. For the lower concentration (Fig. 8a) the initial peaks at $\varphi = 0°$ and $\varphi = 180°$ vanish almost completely (which is accompanied by a temporary drop in the normalized relative integrated intensity) as the electric field is applied. New peaks establish at the final microdomain orientation at $\varphi = 90°$ and $\varphi = 270°$, showing a continuous growth of intensity with time. Intermediate orientations are not observed. For high polymer concentrations (Fig. 8b) a distinctly different behavior is found. The initial peaks continuously shift from their original positions to their final positions

Table 2. Time constants τ of the reorientation of $S_{50}I_{50}{}^{80}$ at different polymer concentrations obtained from least squares fits using (3) ($E = 1\,\mathrm{kV/mm}$, electrode spacing: 2 mm). NG: nucleation and growth, R: grain rotation.

Concentration [wt.%]	τ [sec]	$P_{2,\infty}$	χ^2 [10^{-4}]	dominating mechanism
34.5	0.8	-0.26	0.6	NG
35	5.0	-0.32	1.4	NG
37.5	7.0	-0.34	0.8	NG
40	28.3	-0.33	1.3	NG
42.5	54.0	-0.33	2.4	mixed
45	104	-0.34	3.2	R
47.5	142	-0.26	1.2	R
50	192	-0.31	5.6	R

at $\varphi = 90°$ and $\varphi = 270°$, respectively. The relative integrated intensity of the peaks increases steadily during the shift, i.e. a well-defined anisotropic scattering pattern is observed throughout the entire process. At intermediate concentrations both behaviors coexist. Table 2 shows the prevailing mechanism found for the respective concentration.

Temperature Dependence

A qualitatively similar behavior is found when we follow the reorientation process at different temperatures. For this purpose, a 47.5 wt.% solution was studied between 27°C and 80°C (see Figs. 8c/d). The rather high polymer concentration was chosen to access a large temperature range before reaching the order-disorder transition temperature (T_{ODT}) of the solution. Qualitatively, we find a "rotation" of the scattering pattern from the initial to the final situation at low temperatures, while the scattering pattern "switches" between the two limiting situations at temperatures near T_{ODT}. The results of a quantitative data evaluation are summarized in Table 3. At the lowest temperature (27°C) we measure a time constant of $\tau = 141\,\mathrm{sec}$, which gradually decreases down to 11.5 sec as the temperature is raised up to 80°C. The plateau values of the orientational order parameter $P_{2,\infty}$ seem to show a slight increase from –0.34 to –0.25 with increasing temperature, indicating a decrease of final order.

4.3 Mechanism of Domain Alignment

One of the most important aspects for the understanding of the reorientation behavior of block copolymer microdomains in solution is the knowledge of the underlying mechanisms contributing to the rearrangement of domains. In contrast to in-situ birefringence [13, 14], in-situ SANS [46], and ex-situ

Table 3. Time constants τ of the reorientation of $S_{50}I_{50}{}^{80}$ at different temperatures obtained from least squares fits using (3) ($w_p = 47.5$ wt.%, $E = 1$ kV/mm, electrode spacing: 2 mm). NG: nucleation and growth, R: grain rotation.

Temperature [K]	τ [sec]	$P_{2,\infty}$	χ^2 [10^{-4}]	dominating mechanism
300.15	141	-0.34	4.0	R
308.15	138	-0.28	0.6	R
316.15	106.9	-0.27	3.0	R
324.65	86.5	-0.28	3.8	mixed
333.65	52.5	-0.28	2.3	mixed
343.15	40.6	-0.27	2.5	NG
353.15	11.5	-0.25	0.2	NG

SAXS [10, 12, 47] measurements on block copolymer melts and solutions under shear, which lead to detailed insight into the respective mechanisms, so far only little is known about the microscopic processes during electric field alignment. *In-situ* Synchrotron–SAXS combines the advantages of birefringence (high time resolution) with the detailed and straightforward information about the microscopic order characteristic of scattering methods. Indeed, the SAXS data indicate two distinctly different mechanisms of microdomain reorientation. At low concentrations and at high temperatures, destruction of the initial peaks is followed by a build-up of scattering intensity at the final peak positions. At high concentrations and low temperatures, on the other hand, the scattering pattern merely shifts into new peak positions accompanied by a steady increase of the integrated peak intensities.

These findings point to two different underlying mechanisms responsible for microdomain reorientation in the presence of the electric field. Close to the order/disorder transition (ODT), i.e. at low concentrations and high temperatures, microdomains aligned parallel to the electric field grow at the expense of those aligned parallel to the electrodes. Intermediate orientations, however, are not observed. This behavior matches the notion of the *nucleation and growth* (see Fig. 10a), which has previously been described for microdomain alignment under shear [47] and which was assumed to play a role in earlier electric field experiments [17, 22]. In this case one lamella grows at the expense of another with a significantly different orientation by motion of a tilt boundary (wall defect) between them, leading to a direct transfer of scattering intensity between widely separated azimuthal angles φ. This is indeed observed in Fig. 8a. The integrated scattering intensity exhibits a temporary drop to 65 % of the initial intensity, which coincides with the decrease of the peaks of the initial orientation, indicating the formation of an intermediate structure, e.g. nucleation centers for lamellar grains oriented parallel to the electric field. Their subsequent growth finally leads to an increase of the integrated intensity at later stages of the process.

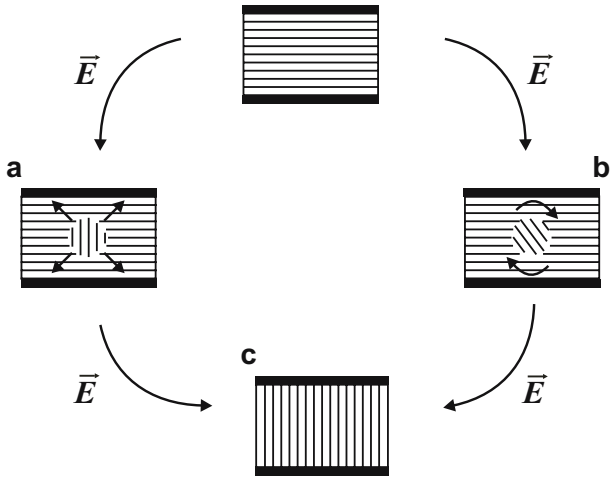

Fig. 10. Schematic representation of lamellar microdomains between two electrodes. (**a**) *Nucleation and growth* and (**b**) *grain rotation* mechanism leading to microdomain orientation parallel to the electric field vector (**c**).

Further away from the ODT, i.e. for high concentrations and low temperatures, the scattering pattern seems to be preserved and merely rotates into the new orientation. This observation points to *grain rotation* as an alternative orientation process (see Fig. 10b). In contrast to the nucleation and growth, microdomain orientations intermediate between the original and the final orientations are observed. At the same time no increase in isotropic scattering intensity is found. We note that, in contrast to the *nucleation and growth*, the integrated scattering intensity in Fig. 8b is found to grow continuously. This indicates an overall growth of domains during the course of the reorientation process. In contrast to mechanical shear fields, the electric field does not impose a preferred direction of grain rotation on the system. The fact that the final orientation parallel to the electric field vector is not fully reached within the experimental time frame is in agreement with the notion that the driving force for grain alignment almost vanishes as the aligned state is approached [17].

The transition from *grain rotation* to *nucleation and growth* can be explained by the fact that close to ODT we expect concentration fluctuations which can be amplified using an external electric field, i.e. the lamellar structure can easily be distorted in the direction of the electric field vector. In addition, the mobility of defects such as wall defects at the grain boundaries is much higher.

In order to further verify the above notion and to gain a more detailed understanding of the governing reorientation mechanisms, two-dimensional dynamic density functional theory simulations have been performed on lamellar block copolymer melts, which were able to reproduce the time evolution

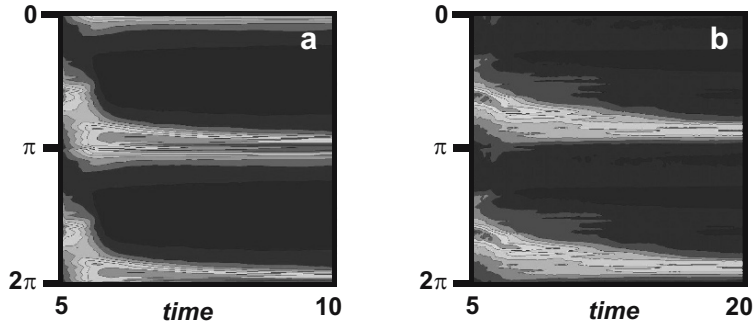

Fig. 11. Fourier transform squared as obtained by Dynamic Density Functional Theory MesoDyn^{TM}-Simulations of lamellar reorientation at dimensionless time t (in units of 1 000 timesteps). (**a**) System close to ODT (mean-field interaction parameter $\varepsilon_{AB} = 6\,\mathrm{kJ/mol}$), (**b**) System further away from ODT (mean- field interaction parameter $\varepsilon_{AB} = 8\,\mathrm{kJ/mol}$). Reprinted with permission from *Macromolecules* [45]. Copyright (2003) American Chemical Society.

of the scattering pattern observed in the experiments [37]. These simulations are based on energetic considerations namely involving electrostatic (i.e. driving force of the process) and interfacial energy (i.e. incompatibility between the block copolymer domains) arguments. The scattering functions calculated from these simulations are shown in Fig. 11 and exhibit the same characteristic features seen in the experimental scattering intensity in Fig. 8. In Fig. 12 we show a typical area of a large simulation box cropped around a newly forming grain for the system close to the ODT (mean-field interaction parameter $\varepsilon_{AB} = 6\,\mathrm{kJ/mol}$) at an electric field strength $\tilde{\alpha} = 0.2$. The initial structure ($t = 5\,000$ timesteps) has first been aligned parallel to the electrodes by shear. Immediately after the application of the electric field (at $t = 5\,100$ timesteps), the lamellae become unstable and exhibit undulations very similar to the ones described by Onuki and Fukuda [48,49], and, eventually, form point-like defects. These serve as nucleation centers for grains with lamellar orientation parallel to the electric field. As the process evolves, new instabilities are formed around the new structure contributing to the growth of the grain with lamellar orientation parallel to the electric field at the expense of all other orientations. Interestingly, the grain seems to grow faster in the direction perpendicular to the electric field vector. On the other hand, the lower left corner of the simulation box shows a different mechanism. Here, the reorientation, initiated by undulations, proceeds via movement of defects (disclination lines) and merely results in a rotation of the lamellar grains. This finding supports our previous notion that the two distinct mechanisms can be simultaneously found in our system. Depending on the degree of phase separation one of the two is dominant. In the presented simulation, as can be seen clearly also from larger simulation boxes, the *nucleation and growth* mechanism prevails [37].

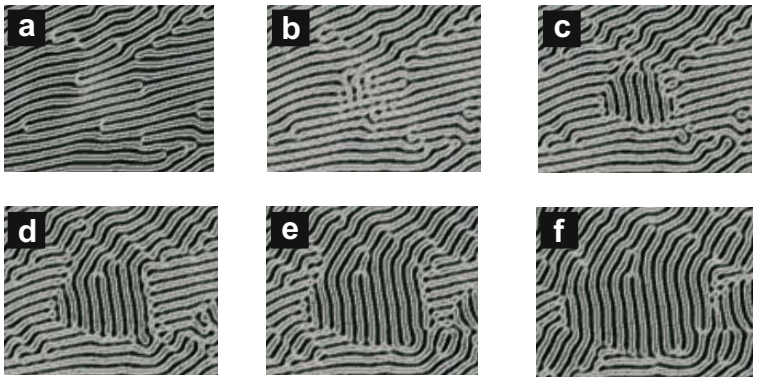

Fig. 12. Real space images of a Dynamic Density Functional Theory MesoDyn^{TM}-Simulation of reorientation close to ODT ($\varepsilon_{AB} = 6\,kJ/mol$) at dimensionless time t (in units of timesteps). (**a**) 5 000, (**b**) 5 100, (**c**) 5 200, (**d**) 5 300, (**e**) 5 400, (**f**) 5 500. The electric field vector runs vertically. Alignment by *nucleation and growth* and *grain rotation* can be distinguished. Reprinted with permission from *Macromolecules* [45]. Copyright (2003) American Chemical Society.

For simulations further away from ODT, we predominantly find that the *grain rotation* mechanism (induced by the movement of well defined defects) governs the reorientation process. The governing mechanisms can be identified clearly from the squared Fourier transforms of the simulated lamellar rearrangement as depicted in Fig. 11 [37] which closely resemble the experimental data shown in Figs. 8a/b as well as Figs. 8c/d. Obviously, for the systems further away from ODT, the energetic cost for additional creation of defects as required for the *nucleation and growth* process is too high compared to the gain in energy from an aligned lamellar phase.

5 Influence of Initial Order

Both lamellar and cylindrical mesophases in block copolymers preferentially align parallel to any boundary surface as such alignment typically decreases the interfacial energy of the structure with the boundary surface. In case of a plate capacitor, these effects counteract the effect of the electric field which points perpendicular to the boundary surfaces. In consequence, a minimum electric field strength (threshold electric field strength) is required to overcome the parallel interfacial alignment [38,50–52]. Moreover, it has been shown that close to the electrodes the parallel alignment may prevail even if the bulk of the film is oriented perpendicular to the interfaces, resulting in a mixed orientation of grains. This even holds for shear aligned samples where the effective forces on the lamellae are much larger than in the electric field case [10, 53]. While the thermodynamics of this competition is widely understood, the in-

fluence of the initial degree of order and initial orientation with respect to the boundary surfaces on the microscopic pathway leading to microdomain reorientation has barely been studied. This is even more surprising given the obvious importance of defect density and initial degree of order for the reorientation process as has been described for shear alignment experiments. *Grain rotation* relies on the movement of individual defects and therefore should strongly depend on the defect density. For the *nucleation and growth* of grains of preferred orientation on the other hand, both structural defects as well as thermal fluctuations may serve as nuclei. Onuki and Fukuda have pointed out that undulation instabilities in lamellae in an oblique electric field will only develop if the angle between the plane of the lamellae and the electric field vector is sufficiently large [48]. Therefore, not only the defect density but also the degree of orientation and the angle between the microdomains and the electric field should be of importance.

In this section, we investigate the influence of the degree of initial order on the microscopic route towards domain alignment. Using different capacitor spacings ($0.3 - 3.8\,\mathrm{mm}$), we control the initial degree of order in the microdomain structures prior to application of the electric field. As we have noted earlier, the lamellae are exposed both to the shear fields occurring during sample preparation (the sample solution is filled into the capacitor via a syringe inserted at one side of the cell with an intake diameter corresponding to the electrode spacing) and to the surface fields favoring parallel alignment of the lamellae [45]. In consequence, the initial microdomain orientation is not random, but preferentially aligned parallel to the capacitor plates. This pre-alignment, which improves with decreasing electrode spacing, can easily be quantified through the orientational order parameter P_2 at $t = 0$ ($P_{2,0}$).

5.1 Reorientation Experiments with Samples of Different Initial Order

We start our discussion with the kinetics of microdomain reorientation as followed in the center of a capacitor filled with a 35 wt.% solution of $S_{50}I_{50}{}^{100}$ in toluene (we note that due to the higher M_w, this sample is further away from ODT than $S_{50}I_{50}{}^{80}$ and is thus expected to exhibit the *grain rotation* mechanism) with the lamellae oriented parallel to the electrodes exhibiting an initial degree of orientational order of $P_{2,0} = 0.50$. Figure 13a shows the time dependence of the azimuthal scattering intensity at $1\,\mathrm{kV/mm}$.

Clearly, at short times an intermediate orientation is observed pointing to grain rotation as the dominant reorientation process. A major part of the scattering intensity is rotated continuously from the initial orientation at $\varphi = 0°$ and $\varphi = 180°$, respectively, to the final orientation at $\varphi = 90°$ and $\varphi = 270°$. This situation changes significantly if we turn to samples with higher initial alignment. In Fig. 13b we show the reorientation behavior of a polymer solution with $P_{2,0} = 0.83$. In contrast to the data shown in Fig. 13a, only

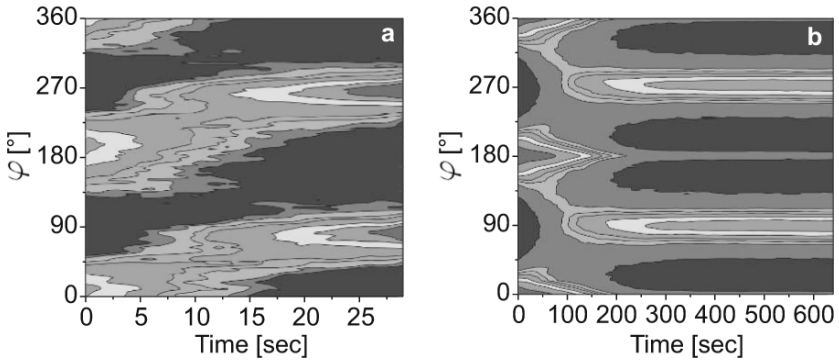

Fig. 13. 3D representation of the azimuthal angular dependence of the scattering intensity for the reorientation of a 35 wt.% solution of $S_{50}I_{50}{}^{100}$ in toluene under an electric field of 1 kV/mm. (**a**) $P_{2,0} = 0.50$; (**b**) $P_{2,0} = 0.83$. Reprinted with permission from *Langmuir* [54]. Copyright (2005) American Chemical Society.

two distinct domain orientations are observed resulting in scattering peaks at $\varphi = 0°$ and $\varphi = 180°$ (initial) and at $\varphi = 90°$ and $\varphi = 270°$ (final).

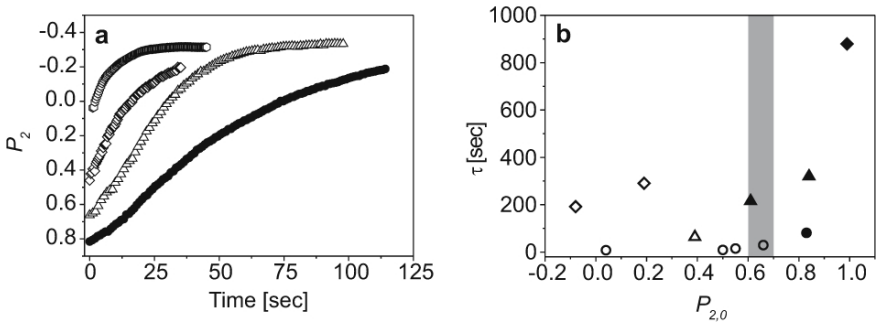

Fig. 14. (**a**) Kinetics of a 35 wt.% solution of $S_{50}I_{50}{}^{100}$ in toluene at 1 kV/mm for different initial degrees of order. Evolution of the orientational order parameter: ⬡: $P_{2,0} = 0.04$ (R), ◇: $P_{2,0} = 0.50$ (R), △: $P_{2,0} = 0.66$ (R), •: $P_{2,0} = 0.83$ (NG). (**b**) Experimental time constants τ as a function of the initial order parameter for solutions of $S_{50}I_{50}{}^{100}$ in toluene at 1 kV/mm: ◇ = 55 wt.%, △ = 50 wt.%, ○ = 35 wt.% from (**a**). Open symbols relate to *grain rotation* as the dominant mechanism, while full symbols refer to *nucleation and growth*. Reprinted with permission from *Langmuir* [54]. Copyright (2005) American Chemical Society.

At intermediate times both orientations coexist, while almost no intermediate orientations are observed and only a negligible portion of the sample rotates. The time dependent plot of the azimuthal scattering intensity clearly shows the switching between the initial and the final orientation. This scattering behavior is indicative of nucleation and growth of grains of the final

orientation. Grain rotation seems to be almost completely suppressed in this situation. It is interesting to quantify the kinetics of reorientation as a function of $P_{2,0}$. In Fig. 14a we show the time dependence of the P_2-values calculated from the raw data according to (1). Fitting a single exponential to the data using (3) yields time constants τ, which increase from $\tau = 7.8\,\mathrm{sec}$ at $P_{2,0} = 0.04$ to as much as $\tau = 81\,\mathrm{sec}$ for $P_{2,0} = 0.83$ (see Table 4). In Fig. 14b, we plot the

Table 4. Time constants τ of the reorientation of $S_{50}I_{50}{}^{100}$ at different values of $P_{2,0}$ obtained from least squares fits using (3) ($w_\mathrm{p} = 35\,\mathrm{wt.\%}$, $E = 1\,\mathrm{kV/mm}$). NG: nucleation and growth, R: grain rotation.

$P_{2,0}$	τ [sec]	dominating mechanism
0.83	81.0	NG
0.66	29.6	R
0.55	15.0	R
0.50	9.0	R
0.04	7.8	R

kinetic data (τ-values) as a function of the initial degree of order $P_{2,0}$ of the microdomains for three different block copolymer solutions. Open symbols relate to *grain rotation* as the dominant mechanism, while full symbols refer to *nucleation and growth*. Only at sufficiently low degrees of order grain rotation is observed. We identify a minimum degree of initial order characterized by a $P_{2,0}$-value between 0.6 and 0.7 (grey area in Fig. 14b), at which we observe a switch from rotation of grains to nucleation and growth. It therefore seems reasonable to assume that the degree of alignment (and in turn: the defect density) has significant influence on the microscopic pathway for microdomain reorientation in the presence of the electric field.

5.2 Simulating Systems with Different Degrees of Initial Order

The above interpretation is strongly corroborated by analysis of the real space data provided by computer simulations. We have performed two-dimensional dynamic self-consistent field simulations on lamellar diblock copolymer melts starting from two different initial conditions. In all cases the microdomain structure was first exposed to a shear field resulting in alignment of the lamellae in a well-defined direction to the electric field vector. Different shearing times and directions (Figs. 15a/b: perpendicular to the electric field vector, Fig. 15c: parallel to the electric field vector) were chosen in order to produce initial states of different degrees of alignment. The copolymer system studied here has mean field interactions $\varepsilon_\mathrm{AB} = 6\,\mathrm{kJ/mol}$. It was found earlier to exhibit nucleation and growth as the dominant reorientation mechanism [37,45].

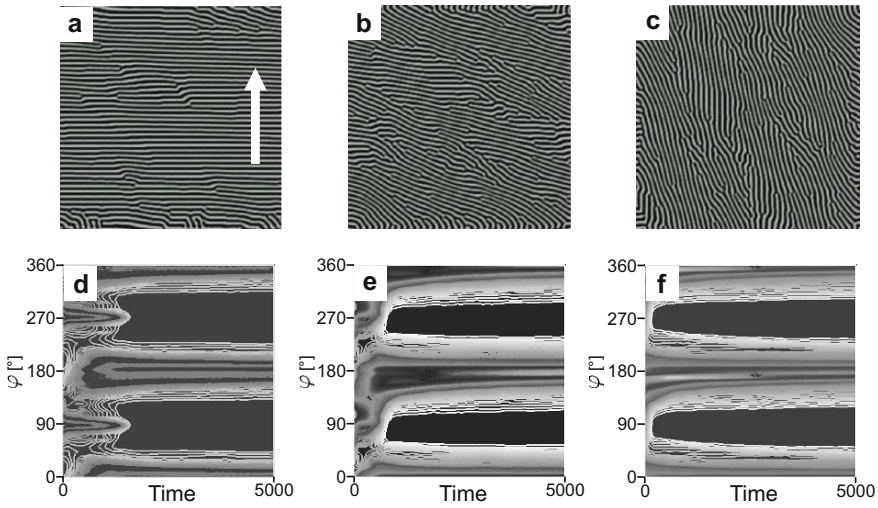

Fig. 15. (**a**–**c**) Self-consistent field theory simulation of initial microdomain structure, prealigned using shear: (**a**) highly aligned sample (7 500 timesteps of shear perpendicular to electric field), (**b**) less aligned sample (2 500 timesteps of shear perpendicular to electric field), (**c**) least aligned sample (2 500 timesteps of shear parallel to electric field). (**d**–**f**) Fourier transform squared of 2D simulated structures at dimensionless time t: (**d**) *Nucleation and growth* mechanism for highly aligned sample, (**e**) Combination of *nucleation and growth* mechanism and some *grain rotation* for the less aligned sample. (**f**) Solely *grain rotation* mechanism for the least aligned sample. The electric field strength is $\tilde{\alpha} = 0.2$. The arrow indicates the direction of the electric field vector. Reprinted with permission from *Langmuir* [54]. Copyright (2005) American Chemical Society.

As the electric field is applied to the microdomain structures described above, a distinctly different behavior is observed depending on the initial degree of alignment parallel to the electrodes. In the highly aligned sample with a largely dominant microdomain orientation perpendicular to the electric field vector (Fig. 15a), the reorientation process is rather slow and proceeds exclusively via nucleation and growth. The scattering functions calculated from these simulations are shown in Fig. 15d and exhibit the same characteristic features seen in the experimental scattering intensity in Fig. 13b. In the less aligned sample (Fig. 15b) reorientation is found to proceed faster and grain rotation increasingly contributes to the reorientation. This is seen in the scattering functions shown in Fig. 15e, which resemble the experimental data found at intermediate $P_{2,0}$-values (Fig. 13a). In the case of a structure even less aligned parallel to the electrodes (Fig. 15c), the same copolymer system exhibits only grain rotation via movement of individual defects perpendicular to the lamellae. The scattering function in Fig. 15f exclusively shows a shift of the peak, with no signs of the nucleation and growth mechanism present. This is very similar to what was observed for the lowest initial degree of order

in this study, $P_{2,0} = 0.04$, as depicted in Fig. 16, showing that the lamellae are less ordered and tilted towards the electric field lines. Obviously, consistent with the theory of Onuki et al. [48], the initial angle between the lamella plane and the electric field vector is not sufficient for the instabilities in the structure to grow. Such instabilities are needed to nucleate grains of an orientation parallel to the external field. In this case, the only possible route to follow for the system is the rotation of grains, as it proceeds via individual defect movement. Moreover, at these intermediate orientations, the electric field induced torque acting on the lamellae increases with increasing lamellar misalignment with respect to the electrodes and reaches its maximum at a tilt angle of 45° [28].

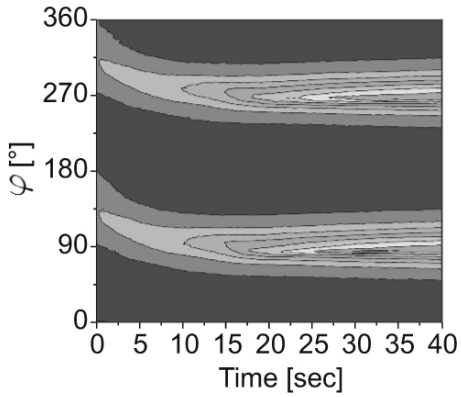

Fig. 16. 3D representation of the azimuthal angular dependence of the scattering intensity for the reorientation of a 35 wt.% solution of $S_{50}I_{50}{}^{100}$ in toluene under an electric field of 1 kV/mm and $P_{2,0} = 0.04$. Reprinted with permission from *Langmuir* [54]. Copyright (2005) American Chemical Society.

A detailed analysis of the real space view of the above described processes reveals that even in the absence of defects in the initial structure in Fig. 15a, grains of the new phase nucleate due to the growth of instabilities. The number of nuclei depends on the initial defect density. The speed of the reorientation processes can be monitored by P_2 plots which qualitatively follow similar trends as the experimental curves as a function of initial alignment. In addition, we have also performed simulations for the copolymer system with mean field interactions $\varepsilon_{AB} = 8\,\mathrm{kJ/mol}$, which was found earlier to reorient via the grain rotation mechanism only [37]. Here, we find a total suppression of the rotation in the better aligned samples. The system is trapped kinetically and only a few defects typical for nucleation and growth are slowly generated. This finding is consistent with the interpretation of the experiments mentioned earlier, that the rotation will be increasingly suppressed when the lamellae are initially oriented more parallel to the electrodes, i.e. with increasing $P_{2,0}$.

Judging from the simulation results, we may indeed assume that the different degrees of initial order are responsible for the observed differences both in the kinetics and in the mechanism of reorientation. As can be seen from Fig. 14b, the process of reorientation becomes slower with increasing alignment and decreasing defect density. This is accompanied by a switch in mechanism from rotation of grains to nucleation and growth. Once the degree of initial order reaches a value of $P_{2,0} > 0.6$, grain rotation seems to be largely suppressed. For $P_{2,0} > 0.7$ grain rotation is no longer observed. Obviously, the number of defects in the microstructure becomes insufficient to support grain rotation by defect movement. Here, structural defects exclusively serve as nucleation centers for new domains. Comparing the rather different time constants for the nucleation and growth process at the highest degrees of initial order, one is led to the assumption that in these cases the number of structural defects is too small to initiate sufficient nucleation centers. Therefore, thermal fluctuations of the lamellae amplified by the external electric field are needed for nuclei to be formed.

In summary, it has been shown in this section that both the reorientation pathway and the reorientation kinetics for lamellar microdomains in an external electric field strongly depend on the degree of order present prior to the application of the field. Samples of the same concentration but different initial order not only exhibit different mechanisms of orientation but also proceed at different rates. We observe consistently that for all systems rotation of lamellae by defect movement is faster than reorientation by nucleation and growth of new domains. Based on our results, we may conclude that above a certain initial orientation parallel to the electrodes the defect density and electric field-induced torque are too low to allow for rotation of grains. In addition, the pressure on the well-aligned lamellae (as already pointed out by Onuki and Fukuda) [48] is larger than for less aligned samples and therefore leads to undulation instabilities which finally serve as nucleation centers for the growth of grains oriented parallel to the external electric field. This leads to a switch in orientation mechanism with increasing initial microdomain orientation from rotation to nucleation and growth.

6 Outlook

In this chapter, we have shown that polymer concentration, dielectric contrast of the blocks and temperature as well as the initial degree of order in the system are some of the key parameters governing the *electric field-induced* alignment of block copolymer microdomains from *solution*. The interplay of these parameters determines the kinetics as well as the mechanisms of the overall orientation process. Gaining control over these factors turns electric fields into a powerful tool to direct block copolymer self-assembly.

While the microscopic mechanisms and their determinig factors seem clear, the underlying mechanism at the level of individual macromolecules or even

monomer units remains elusive. Therefore, one future area of research in this field could be concerned with the investigation of conformational changes of the block copolymer chains induced by the external electric field, e.g. a significant stretching or compression of the Gaussian chains.

In addition, it has been anticipated theoretically, that a strong electric field may induce a shift in the order-disorder transition temperature (T_{ODT}) at field strengths close to the dielectric breakdown of polymeric materials ($E > 30\,\mathrm{kV/mm}$) [55, 56]. Such effects have already been found to be induced by shear fields in lamellar block copolymer solutions [46]. For electric fields, Wirtz and Fuller reported on field-induced structures in homopolymer solutions near the critical point [57, 58]. Tsori et al. recently found that electric field gradients of moderate field strength ($4\,\mathrm{kV/mm}$ at $1\,\mathrm{kHz}$) lead to demixing of blends consisting of low molecular weight PDMS and squalane [59]. So far, the above described phenomena and their impact on the morphology formation have not been studied for block copolymers.

All these investigations will contibute to a deeper understanding of the interactions of polymer microstructures with external electric fields thus enhancing the high potential of the described directed self-assembly processes for future technological applications of block copolymer templates such as data storage, nanoelectronics or lab-on-a-chip devices [1].

Acknowledgement. I would like to thank all coworkers from the University of Bayreuth and the European Synchrotron Radiation Facility (ESRF) who have contributed to the work presented in this chapter, in particular: Volker Abetz, Hubert Elbs, Franz Fischer, Helmut Hänsel, Armin Knoll, Georg Krausch, Axel H.E. Müller, Kristin Schmidt, Frank Schubert, Volker Urban, Thomas M. Weiss, and Heiko Zettl. In addition, I would like to acknowledge Agur Sevink and Andrei Zvelindovsky for performing the MesoDyn$^{\mathrm{TM}}$ simulations.

This work is financially supported by the ESRF and the Deutsche Forschungsgemeinschaft (DFG) in the framework of the Sonderforschungsbereich SFB 481 (Teilprojekt A2). Finally, I am grateful to Wolfgang Häfner for patiently introducing me to LaTeX and much helpful technical advice. Moreover, I thank him, Kristin Schmidt and Heiko Schoberth for proof-reading of the manuscript.

References

1. C. Park, J. Yoon, and E. L. Thomas. *Polymer*, 44:6725–6760, 2003.
2. F. S. Bates and G. H. Fredrickson. *Annu. Rev. Phys. Chem.*, 41:525–557, 1990.
3. F. S. Bates and G. H. Fredrickson. *Physics Today*, 52:32–38, 1999.
4. V. Abetz and R. Stadler. *Macromol. Symp.*, 113:19–26, 1997.
5. S. Ludwigs, A. Böker, V. Abetz, A. H. E. Müller, and G. Krausch. *Polymer*, 44:6815–6823, 2003.
6. R. J. Albalak, E. L. Thomas, and M. S. Capel. *Polymer*, 38:3819–3825, 1997.
7. T. L. Morkved, P. Wiltzius, H. M. Jeager, D. G. Grier, and T. A. Witten. *Appl. Phys. Lett.*, 64:422–4, 1994.

8. W. A. Lopes and H. M. Jaeger. *Nature*, 414:735–738, 2001.
9. A. Keller, E. Pedemonte, and F. M. Willmouth. *Nature*, 225:538, 1970.
10. K. I. Winey, S. S. Patel, R. G. Larson, and H. Watanabe. *Macromolecules*, 26:4373–4375, 1993.
11. R. J. Albalak and E. L. Thomas. *J. Polym. Sci. Polym. Phys.*, 32:341–350, 1994.
12. U. Wiesner. *Macromol. Chem. Phys.*, 198:3319–3352, 1997.
13. Z. R. Chen, J. A. Kornfield, S. D. Smith, J. T. Grothaus, and M. M. Satkowski. *Science*, 277:1248–1253, 1997.
14. Z. R. Chen and J. A. Kornfield. *Polymer*, 39:4679–4699, 1998.
15. T. Hashimoto, J. Bodycomb, Y. Funaki, and K. Kimishima. *Macromolecules*, 32:952–954, 1999.
16. J. M. Serpico, G. E. Wnek, S. Krause, T. W. Smith, D. J. Luca, and A. Vanlaeken. *Macromolecules*, 25:6373–6374, 1992.
17. K. Amundson, E. Helfand, X. Quan, and S. D. Smith. *Macromolecules*, 26:2698–2703, 1993.
18. T. Thurn-Albrecht, J. Schotter, G. A. Kastle, N. Emley, T. Shibauchi, L. Krusin-Elbaum, K. Guarini, C. T. Black, M. T. Tuominen, and T. P. Russell. *Science*, 290:2126–2129, 2000.
19. T. Thurn-Albrecht, J. DeRouchey, T. P. Russell, and R. Kolb. *Macromolecules*, 35:8106–8110, 2002.
20. A. Böker, A. Knoll, H. Elbs, V. Abetz, A.H. E. Müller, and G. Krausch. *Macromolecules*, 35:1319–1325, 2002.
21. A. Böker, H. Elbs, H. Hänsel, A. Knoll, S. Ludwigs, H. Zettl, V. Urban, V. Abetz, A. H. E. Müller, and G. Krausch. *Phys. Rev. Lett.*, 89:135502, 2002.
22. K. Amundson, E. Helfand, D. D. Davis, X. Quan, S. S. Patel, and S. D. Smith. *Macromolecules*, 24:6546–6548, 1991.
23. T. L. Morkved, M. Lu, A. M. Urbas, E. E. Ehrichs, H. M. Jaeger, P. Mansky, and T. P. Russell. *Science*, 273:931–933, 1996.
24. T. L. Morkved, W. A. Lopes, J. Hahm, S. J. Sibener, and H. M. Jaeger. *Polymer*, 39:3871–3875, 1998.
25. P. Mansky, J. DeRouchey, T. P. Russell, J. Mays, M. Pitsikalis, T. Morkved, and H. Jaeger. *Macromolecules*, 31:4399–4401, 1998.
26. T. Thurn-Albrecht, J. DeRouchey, T. P. Russell, and H. M. Jaeger. *Macromolecules*, 33:3250–3253, 2000.
27. J. Brandrup and E. H. Immergut. *Polymer Handbook*. Wiley & Sons, New York, 4th edition, 1998.
28. L. D. Landau and E. M. Lifshitz. *Electrodynamics of Continuous Media*. Pergamon, Oxford, 1960.
29. T. Thurn-Albrecht, R. Steiner, J. DeRouchey, C. M. Stafford, E. Huang, M. Bal, M. Tuominen, C. J. Hawker, and T. P. Russell. *Adv. Mater.*, 12:787–790, 2000.
30. A. Böker, A. H. E. Müller, and G. Krausch. *Macromolecules*, 34:7477–7488, 2001.
31. H. Schmalz, A. Böker, R. Lange, G. Krausch, and V. Abetz. *Macromolecules*, 34:8720–8729, 2001.
32. G. J. A. Sevink, A. V. Zvelindovsky, B. A. C. van Vlimmeren, N. M. Maurits, and J. G. E. M. Fraaije. *J. Chem. Phys.*, 110:2250–2256, 1999.
33. B. A. C. van Vlimmeren, N. M. Maurits, A. V. Zvelindovsky, G. J. A. Sevink, and J. G. E. M. Fraaije. *Macromolecules*, 32:646–656, 1999.

34. G. H. Fredrickson and L. Leibler. *Macromolecules*, 22:1238–1250, 1989.
35. A. Knoll, A. Horvat, K. S. Lyakhova, G. Krausch, G. J. A. Sevink, A. V. Zvelindovsky, and R. Magerle. *Phys. Rev. Lett.*, 89:035501, 2002.
36. A. Onuki. *Phase Transition Dynamics*. Univ. Press, Cambridge, 2002.
37. A. V. Zvelindovsky and G. J. A. Sevink. *Phys. Rev. Lett.*, 90:049601, 2003.
38. K. S. Lyakhova, A. V. Zvelindovsky, and G. J. A. Sevink. Slow dynamics in complex systems. In M. Tokuyama and I. Oppenheim, editors, *AIP Conference Proceedings*, volume 708, pages 217–220, 2004.
39. A. V. Zvelindovsky, G. J. A. Sevink, B. A. C. van Vlimmeren, N. M. Maurits, and J. G. E. M. Fraaije. *Phys. Rev. E*, 57:R4879–R4882, 1998.
40. S. H. Anastasiadis, T. P. Russell, and S. K. Satija. *Phys. Rev. Lett.*, 62:1852, 1989.
41. A. Böker, K. Schmidt, A. Knoll, H. Zettl, H. Hänsel, V. Urban, V. Abetz, and G. Krausch. *Polymer*, 47:849–857, 2006.
42. A. Kozak, G. P. Simon, and G. Williams. *Polymer Commun.*, 30:102–5, 1989.
43. R. Yamaguchi and S. Sato. *Japanese Journal of Applied Physics Part 2: Letters*, 33:4007, 1994.
44. E. Schäffer, T. Thurn-Albrecht, T. P. Russell, and U. Steiner. *Nature*, 403:874–877, 2000.
45. A. Böker, H. Elbs, H. Hänsel, A. Knoll, S. Ludwigs, H. Zettl, A. V. Zvelindovsky, G. J. A. Sevink, V. Urban, V. Abetz, A. H. E. Müller, and G. Krausch. *Macromolecules*, 36:8078–8087, 2003.
46. N. P. Balsara and B. Hammouda. *Phys. Rev. Lett.*, 72:360–363, 1994.
47. D. L. Polis, S. D. Smith, N. J. Terrill, A. J. Ryan, D. C. Morse, and K. I. Winey. *Macromolecules*, 32:4668–4676, 1999.
48. A. Onuki and J. Fukuda. *Macromolecules*, 28:8788–8795, 1995.
49. J. Fukuda and A. Onuki. *J. Phys. II*, 5:1107–13, 1995.
50. T. Xu, C. J. Hawker, and T. P. Russell. *Macromolecules*, 36:6178–6182, 2003.
51. T. Xu, Y. Q. Zhu, S. P. Gido, and T. P. Russell. *Macromolecules*, 37:2625–2629, 2004.
52. Y. Tsori, F. Tournilhac, and L. Leibler. *Macromolecules*, 36:5873–5877, 2003.
53. J. H. Laurer, B. S. Pinheiro, D. L. Polis, and K. I. Winey. *Macromolecules*, 32:4999–5003, 1999.
54. K. Schmidt, A. Böker, H. Zettl, F. Schubert, H. Hänsel, F. Fischer, T. M. Weiss, V. Abetz, A. V. Zvelindovsky, G. J. A. Sevink, and G. Krausch. *Langmuir*, 21:11974, 2005.
55. E. Gurovich. *Macromolecules*, 27:7339–62, 1994.
56. E. Gurovich. *Phys. Rev. Lett.*, 74:482–5, 1995.
57. D. Wirtz, K. Berend, and G. G. Fuller. *Macromolecules*, 25:7234–7246, 1992.
58. D. Wirtz and G. G. Fuller. *Phys. Rev. Lett.*, 71:2236–2239, 1993.
59. Y. Tsori, F. Tournilhac, and L. Leibler. *Nature*, 430:544–547, 2004.